*buildings*

MDPI

*Article*

# Effect of Recycled Concrete Aggregates on the Concrete Breakout Resistance of Headed Bars Embedded in Slender Structural Elements

**Maurício de Pina Ferreira [1,*], Karoline Dantas dos Santos [1], Manoel José Mangabeira Pereira Filho [2] and Luciana de Nazaré Pinheiro Cordeiro [1,*]**

[1] Institute of Technology, Federal University of Para, Belem 66075-110, Brazil; kds@ufpa.br
[2] Faculty of Civil Engineering, Tucuruí Campus, Federal University of Para, Tucuruí 68464-000, Brazil; manoelmangabeira@hotmail.com
* Correspondence: mpina@ufpa.br (M.d.P.F.); lucianapc@ufpa.br (L.d.N.P.C.); Tel.: +55-91-3201-7679 (M.d.P.F.)

**Abstract:** Recycled concrete aggregates are potentially interesting for the precast concrete industry as they provide a new use for high-quality waste from its products' life cycle. In precast concrete structures, it is common to use headed bars in several connection types between structural members. This paper presents the results of experimental tests to investigate the impact of replacing coarse natural aggregates with coarse recycled concrete aggregates in the concrete breakout strength of cast-in headed bars embedded in slender structural elements. Results of 12 tests on 16 mm headed bars embedded in 500 × 200 × 900 mm concrete members with an effective embedment depth of 110 mm are presented. The percentage of replacement of natural aggregates by recycled concrete aggregates was 0%, 30%, and 100%, and the flexural reinforcement ratio of the structural elements varied from 0.5% to 3.5%. The behavior and strength of the tested specimens are discussed, and comparisons with theoretical strength estimates are presented. The results showed that the concrete breakout strength of the headed bars was not affected by the use of recycled concrete aggregates and that the flexural reinforcement ratio significantly impacts the load-carrying capacity of the headed bars as they control the crack widths before failure.

**Keywords:** recycled concrete; recycled aggregate; concrete breakout; headed bars

check for updates

**Citation:** Ferreira, M.d.P.; Santos, K.D.d.; Pereira Filho, M.J.M.; Cordeiro, L.d.N.P. Effect of Recycled Concrete Aggregates on the Concrete Breakout Resistance of Headed Bars Embedded in Slender Structural Elements. *Buildings* **2024**, *14*, 2102. https://doi.org/10.3390/buildings14072102

Academic Editor: Marco Bonopera

Received: 24 April 2024
Revised: 11 June 2024
Accepted: 12 June 2024
Published: 9 July 2024

**Copyright:** © 2024 by the authors. Licensee MDPI, Basel, Switzerland. This article is an open access article distributed under the terms and conditions of the Creative Commons Attribution (CC BY) license (https://creativecommons.org/licenses/by/4.0/).

## 1. Introduction

The production of concretes with the substitution of natural coarse aggregate (NCA) by coarse recycled concrete aggregate (RCA) contributes to the reuse of construction waste, presenting unique opportunities within the precast concrete industry. By utilizing rejected or discarded precast elements, besides using concrete production waste, the recycled concrete aggregates produced have high quality, known origin, and low levels of contaminants due to production controls. Moreover, by integrating RCA production within the precast concrete cycle, transport costs can be eliminated, creating a favorable economic scenario.

Although there is no consensus about the impact caused by the substitution of natural aggregates with recycled concrete aggregates on the mechanical properties of concrete, research like those from Omary, S et al. [1], Koper, A et al. [2], Pedro, D et al. [3], Salesa, A et al. [4], Fiol, F et al. [5], Bai, G et al. [6], and Berredjem, L et al. [7] suggest that maintaining levels comparable to those of conventional concrete is feasible. However, the mechanical properties of concrete with recycled concrete aggregates are fundamentally related to the quality of the concrete waste, the ratio of substitutd aggregates, and the improvement of the granulometric curves.

Despite the high potential of replacing NCA with RCA, the use of RCA for structural purposes is restricted. RCA is commonly used to produce non-structural concretes in applications such as filling materials, pavement bases and sub-bases, and seal cinder blocks.

For structural applications, the literature indicates divergent conclusions regarding the impact of replacing NCA with RCA.

Experimental investigations on the flexural and shear strength of reinforced concrete structural elements conducted by Seara-Paz, S et al. [8] and Huanf, Y et al. [9] identified no significant reductions in terms of performance and resistance due to substituting NCA with RCA. In contrast, studies such as those by Katkhuda, H and Shatarat, N [10] and Malesev, M et al. [11] present opposite conclusions.

Cast-in headed bars are commonly used to transfer forces in connections between precast concrete structural elements. Applications include column–foundation, beam–column, beam–wall, and beam–beam joints, among others, where they are subject to axial tensile or compressive forces, shear forces, or a combination of axial and shear forces. When subjected to tensile stress, these connections can fail by concrete breakout. Standard design methods, such as ACI 318 [12] and *fib* Bulletin 58 [13], assume that the concrete breakout strength of a concrete cone mainly depends on the effective embedment of the anchor, the compressive strength of the concrete, and the degree of concrete cracking around the steel anchor.

The recommendations provided [12,13] are based on experimental tests on cast-in anchors embedded in thick concrete members, most of them without surface reinforcement and with induced cracks, whose widths ranged from 0.3 mm to 0.5 mm. These tests are representative of some design cases, such as base–column connections, as shown in Figure 1a. However, there are design situations where headed deformed bars are embedded in the tension zone of slender structural members, as shown in Figure 1b.

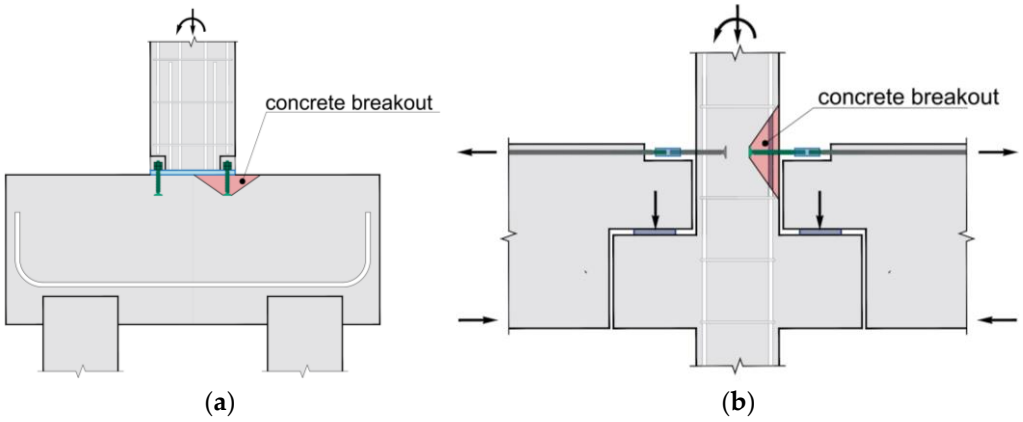



**Figure 1.** Use of headed bars to transfer tensile forces in precast concrete connections: (**a**) column-to-deep pile cap foundation connection and (**b**) semi-rigid beam-to-column connection.

Tensile tests on headed bars embedded in thick concrete members led to the conclusion that surface reinforcement does not impact the concrete breakout strength of headed bars (see Eligehausen, R et al., [14]). Nevertheless, Nilsson, M et al. [15] demonstrated that surface reinforcement could enhance the load-carrying capacity of anchor bolts based on their quantity and positioning. Additionally, Ferreira, M et al. [16] and Santana, P.F et al. [17] showed that for slender reinforced concrete members, the flexural reinforcement ratio affects the concrete breakout strength of headed bars as they are able to control the crack widths before failure.

In this context, this paper presents the results from 12 experimental tests performed to investigate the effect of the substitution rate of NCA with RCA on the concrete breakout strength of cast-in headed bars. The main variable of these tests was the amount of NCA replaced by RCA, with values of 0% (as a reference), 30%, and 100%. The secondary variable was the flexural reinforcement ratio of the concrete elements. Four rates of variation were assumed for the flexural reinforcement, which covered the interval of usual values for the minimum and maximum reinforcement rates allowed by the design standards. The objectives were to determine if the RCA substitution rate can affect the concrete breakout

strength of headed bars and to assess whether this variation changes as a function of the cracking degree of concrete.

## 2. Literature Review

### *2.1. Concrete with Recycled Concrete Aggregates*

The reuse of construction waste offers a promising opportunity for developing sustainable construction. Integrating alternative materials into cement mixtures can mitigate the environmental impacts of the construction process. While research on the behavior and resistance of structural elements employing recycled aggregates remains limited, it is widely acknowledged that the utilization of such aggregates affects the mechanical properties of concrete.

Elsayed, S. R. et al. [18] revealed that the complete substitution of natural coarse aggregates (NCA) with recycled coarse aggregates (RCA) had an adverse impact on the ultimate moment capacity, ultimate shear strength, initial stiffness, ductility, and toughness of tested beams. Additionally, Rahal, K et al. [19] investigated the shear strength of beams without stirrups and reported a reduction in the shear strength of reinforced concrete beams containing recycled aggregates. These results were attributed to recycled aggregates' physical characteristics, making them more brittle than natural aggregates.

The performance and durability of concrete recycled aggregate are directly influenced by the origin of the concrete, the substitution proportion, and the degree of waste saturation [20,21]. Concrete recycled aggregates have mostly interconnected pores, which affect their absorption capacity. Additionally, they are heterogeneous materials with points of fragility, such as the transition zone of both old and new concrete. However, proper dosing and material processing can overcome these limiting points.

Studies indicate that using mineral additives improves pore structure, favoring the formation of additional secondary CSH [22,23]. When combined with chemical additives, concrete with a denser microstructure is produced, promoting refinement of the pores. Other researchers suggest treating the concrete with $CO_2$ before use, as this action can produce $CaCO_3$, which strengthens the structure of micropores, making them denser and improving the material's microstructure [23]. Control of the production process can minimize these effects; for example, immersing alternative aggregates in double or triple mixtures can enhance weak points. Pre-saturation can ensure consistency in the water-to-cement ratio.

According to Behera, M et al. [24], RCA is obtained by crushing concrete elements, resulting in particles with rough surfaces and irregular shapes. Hanse, T.C [25], Casuccio, M [26], and Mcneil, K. and Kang, T.H. [20] noted that the main properties of RCA include density, porosity, water absorption, aggregate shape, particle size composition, and abrasion resistance and showed that these properties are closely linked to the quantity and quality of the old mortar adhered to the grains.

Padmini, A. K et al. [27], Akbarnezhad, A. [21], Behera, M et al. [24], Omary, S. et al. [1], and Saravanakumar, P. et al. [22] showed that higher proportions of mortar with a lower density can decrease the bulk density and increase water absorption compared to the aggregate. Bai, G. et al. [6] and Koper, A [2] reported that reductions in the water absorption of RCA can be obtained by selecting higher-strength concretes. According to Cabral et al. [28], Mcneil, K. and Kang, T.H [20], Behera, M et al. [24], and Kubissa, W. [23], the compressive strength of concrete with RCA is strongly related to the properties and amounts of the recycled aggregates used. Paine, K. and Dhir, R. [29] and Limbachiya, M.C et al. [30] reported that for practical purposes, the use of up to 30% RCA had slight effects on the compressive strength of concrete.

Çakir, O [31] and Silva, R [32] reported that the tensile strength of concrete with the addition of recycled concrete aggregates was lower than that of conventional concrete, but that the reduction in the tensile strength can be controlled through the appropriate selection of recycled aggregates with the best particle size distribution and appropriate mixing processes. Paine, K. and Dhir, R [29] observed that the addition of up to 30% RCA

had little effect on the modulus of elasticity of concretes; for 100% RCA substitutions, Xiao, J et al. [33] and Gomes, M. and de Brito, J [34] found a 20 to 40% reduction in the modulus of elasticity. Behera, M et al. [24] attributed this decrease in the modulus of elasticity to the intrinsic porosity of the mortar adhered to the grains and the presence of voids and cracks caused by the aggregate processing.

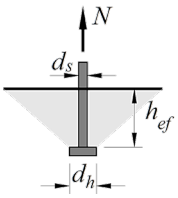
### *2.2. Concrete Breakout Strength*

Headed anchors are usually used to transfer forces between structural elements. These devices are differentiated by the installation mode and the force transfer mechanism and mainly depend on the nominal embedment ($h_{ef}$). According to ACI 318 [12], $h_{ef}$ is the depth required to install the anchor through which the transfer of forces to the concrete is developed. The transfer mechanism for cast-in headed anchors subjected to tensile forces mainly occurs by mechanical anchoring promoted by the contact between the anchor head and the concrete. In terms of the ultimate limit state of steel anchors embedded in concrete, *fib* Bulletin 58 [13] indicates five failure modes: concrete breakout or concrete cone failure, yielding of the steel anchor, lateral detachment, pull-out, and concrete splitting. According to Eligehausen, R et al. [14], concrete breakout failure is characterized by the formation of a crack circumferential to the anchor. This failure mode occurs due to the accumulation of stresses in the anchor's head, which generates tensile stresses in the concrete and causes the material to crack. Concrete breakout occurs when stresses exceed the tensile strength of concrete. Knowledge of the failure plane is essential to determine the tensile strength of the anchor. Eligehausen, R. and Sawade, G. [35], Eligehausen, R. et al. [36], Ozbolt, J. and Eligehausen, R [37], Ferreira, M. et al. [16], and Di Nunzio, G. et al. [38] reported that the failure crack occurred at 35° in relation to the head of the anchor and that this angle was independent of the effective embedment.

Without considering edge effects or the effects of adjacent anchors, the characteristic tensile strength of an anchor for concrete cone failure can be calculated using Equation (1), where $k_1$ is a constant that considers the cracking state of the concrete, *fc* is the compressive strength of the concrete, and $h_{ef}$ is the effective embedment length of the anchor. Table 1 summarizes the theoretical parameters of *fib* Bulletin 58 [13] and ACI 318 [12].

$$N_u = k_1 \cdot \sqrt{f_c} \cdot h_{ef}^n \quad (1)$$

**Table 1.** Theoretical parameters used for strength estimates.

| Notation | Factor k | fib Bull. 58 | ACI 318-19 |
|---|---|---|---|
|  | $k_1$ for uncracked concrete | 12.7 | 12.5 for hef < 280 mm<br>4.9 for 280 mm ≤ hef < 635 mm |
| | $k_1$ for cracked concrete | 8.9 | 10.0 for hef < 280 mm<br>3.9 for 280 mm ≤ hef < 635 mm |
| | $n$ | 3/2 | 3/2 hef < 280 mm<br>5/3 for 280 mm ≤ hef < 635 mm |

The design approaches presented by fib Bulletin 58 [13] and ACI 318 [12] are based on semi-empirical models that take into account only the concrete's compressive strength, the effective embedment depth of the steel anchor, and a constant factor that accounts for the concrete's cracking degree. As reported by Karmokar, T et al. [39], the maximum diameter and type of coarse aggregate used in concrete may affect the concrete breakout strength and should be considered by design approaches.

Ferreira, M et al. [16] present the results of tests on cast-in headed bars embedded in slender reinforced concrete members with different flexural reinforcement ratios. The experimental results indicated that increments in the flexural reinforcement ratio positively

impacted the head bars' concrete breakout strength as they controlled the crack widths before failure, which the design approaches presented in Table 1 did not consider.

## 3. Experimental Program

### *3.1. Materials*

The cement used in the concrete production was CP V-ARI RS, a rapid hardening and sulfate-resisting Portland cement commonly used in Brazil. The concrete mixtures used natural quartz sand (NQS) as fine aggregates. Crushed basalt gravel with a maximum diameter of 25 mm was used as natural coarse aggregate (NCA).

The coarse recycled concrete aggregates (RCAs) were produced from cylindric samples used to test the compressive strength of concrete. These tests were carried out in the Laboratory of Construction Materials of the Federal University of Para, and the samples were selected to cover concrete strengths ranging from 20 MPa to 40 MPa.

A jaw crusher was used to process the concrete waste and produce the recycled aggregates. The size of the coarse aggregates was controlled to be in the fraction size of 4.8 mm to 25 mm. Figure 2 presents the granulometric curve of the aggregates used to produce the concrete of the tested structural members, and their physical properties are presented in Table 2.

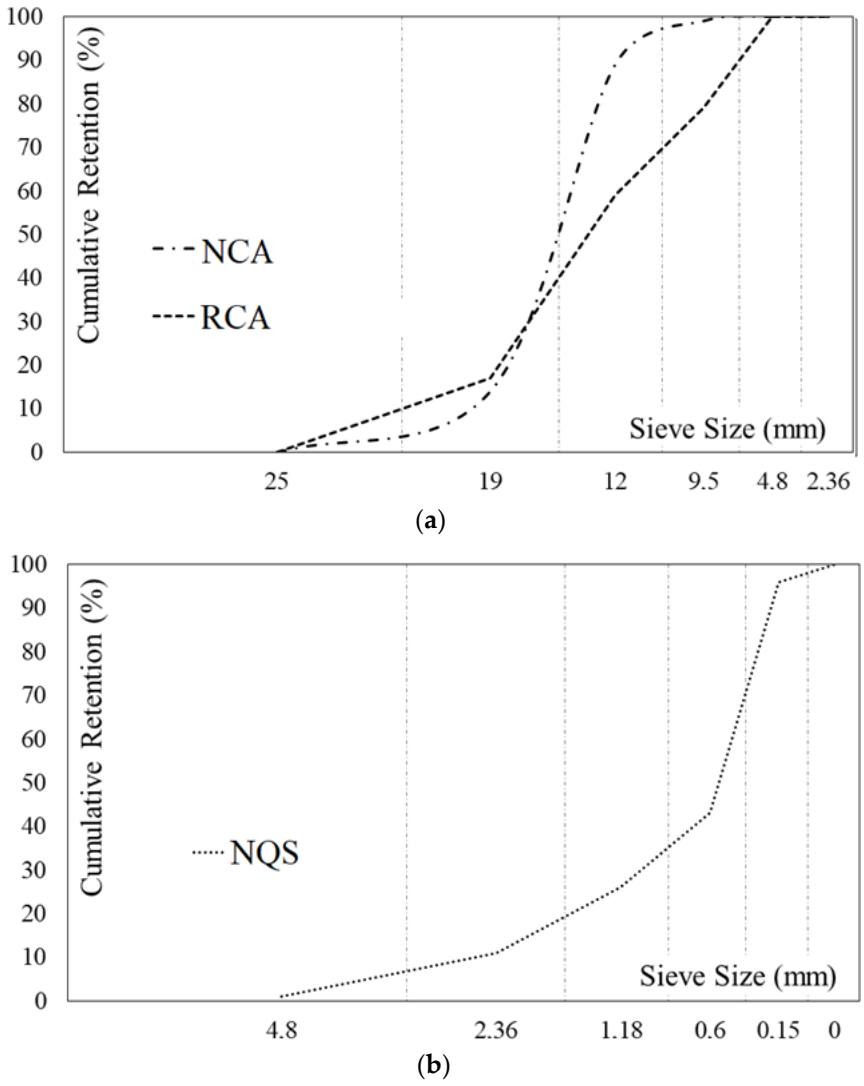



**Figure 2.** Granulometric curves of the aggregates: (**a**) coarse aggregates and (**b**) fine aggregates.

**Table 2.** Physical properties of the aggregates.

| | Natural Quartz Sand | Natural Coarse Aggregate | Recycled Concrete Aggregate |
|---|---|---|---|
| Fineness modulus | 2.61 | 7.00 | 6.96 |
| Maximum aggregate size (mm) | 4.80 | 25.4 | 25.4 |
| Density (g/cm$^3$) | 2.61 | 2.62 | 2.66 |
| Bulk density (g/cm$^3$) | 1.67 | 1.34 | 1.11 |

### 3.2. Concrete Production

The concrete mixtures were defined using Helene. P. and Terzian's IPT/EPUSP method (see reference [40]). Tests were conducted to define the concrete mix to meet the established workability and resistance requirements. The concrete slump was defined as 150 mm ± 20 mm, and the characteristic compressive strength of concrete was set as 30 MPa at 28 days. Table 3 presents the concrete mix for 0%, 30%, and 100% RCA, where (m) is the unit mass, (a) is the unit proportion of fine aggregates, (p) is the proportion of natural coarse aggregates, (pRCA) is the proportion of coarse recycled concrete aggregates, (w/c) is the water-cement ratio, and (C) is the cement consumption.

**Table 3.** Proportions of concrete mixtures.

| % of RCA | Unit Mix Proportion | | | | W/C | C |
|---|---|---|---|---|---|---|
| | m | a | p | pRCA | | (kg/m$^3$) |
| 0 | 5.3 | 2.21 | 3.09 | - | 0.59 | 342.5 |
| 30 | 5.1 | 2.11 | 2.09 | 0.9 | 0.60 | 343.8 |
| 100 | 5.2 | 2.16 | - | 3.04 | 0.65 | 337.2 |

In the mixtures with RCA, the wastes were not pre-saturated because the production process was very close to that of the conventional methodology of concrete manufacturing.

### 3.3. Characteristics of Reinforced Concrete Specimens

The experimental program consisted of 12 tests in headed bars embedded in slender reinforced concrete structural members. The program was subdivided into three series of tests with four prisms each. For each series, different percentages of RCA were substituted for the NCA, and within each test series, different flexural reinforcement rates were assigned. The dimensions of the concrete elements were 500 × 200 × 900 mm, with RCA amounts of [0; 100]%, concrete compressive strengths $f_c$ of [25.2; 27.2] MPa, tensile strengths $f_{ct}$ of [2.7; 3.2] MPa, moduli of elasticity $E_{ci}$ of [16.7; 20.8] GPa, and flexural reinforcement rates ρ$f$ of [0.5; 3.5] %. The diameter of the shank $d_s$ and of the head $d_h$ of the headed bars were 16 and 51 mm, respectively. The effective embedment $h_{ef}$ of the headed bars was 110 mm. The arrangement of the flexural and shear reinforcements is shown in Figure 3, and the nomenclature and general characteristics of the tested specimens are presented in Table 4. All tested specimens were designed to fail due to concrete breakout, and design checks were performed according to *fib* Bulletin 58 [13].

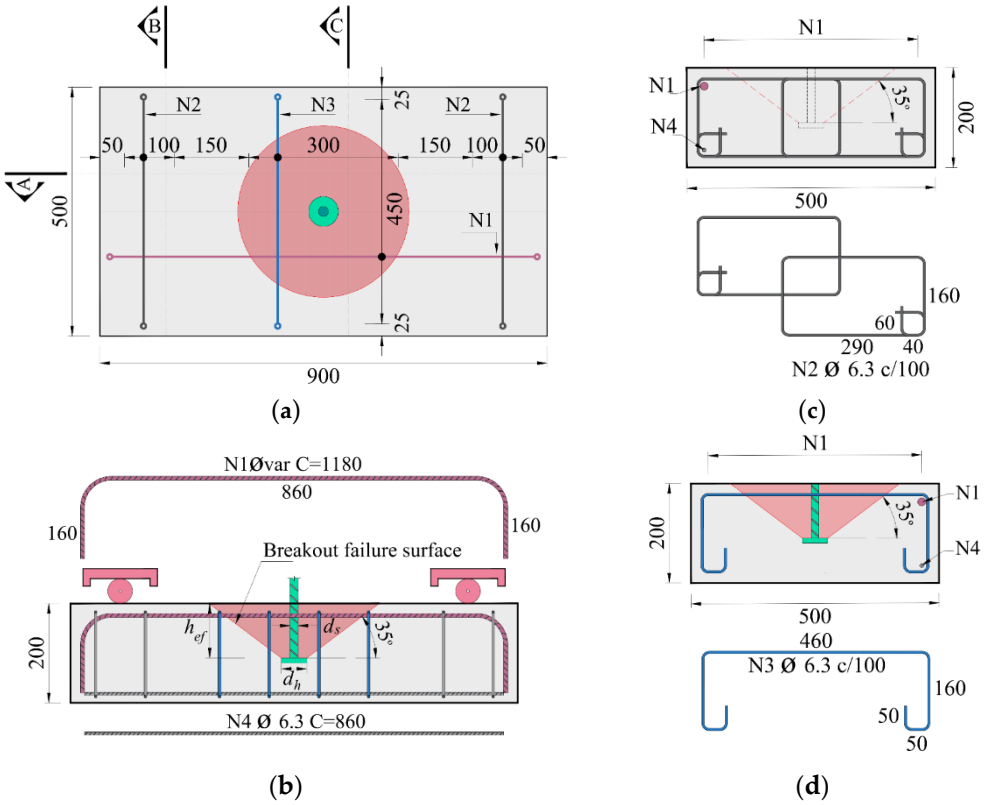



**Figure 3.** General details of the flexural and shear reinforcement of the tested specimens: (**a**) plain view, (**b**) Section A-A, (**c**) Section B-B, and (**d**) Section C-C.

**Table 4.** Characteristics of the tested specimens.

| Specimen | % of RCA | $d$ mm | $h_{ef}$ mm | Flexural Reinforcement | | | | | Concrete | | |
|---|---|---|---|---|---|---|---|---|---|---|---|
| | | | | $n_f$ N1 | $Ø_f$ (mm) | $f_{y,f}$ (MPa) | $E_f$ (GPa) | $\rho_f$ (%) | $f_c$ (MPa) | $f_{ct}$ (MPa) | $E_{ci}$ (GPa) |
| F1-0.5-0 | 0 | 175 | 119 | 6 | 10.0 | 590.3 | 198 | 0.5 | 27.1 | 3.2 | 20.3 |
| F2-1.1-0 | | 174 | 115 | 8 | 12.5 | 590.3 | 196 | 1.1 | 25.2 | 3.0 | 20.8 |
| F3-2.2-0 | | 170 | 120 | 6 | 20.0 | 506.7 | 190 | 2.2 | 27.1 | 3.2 | 20.3 |
| F4-3.5-0 | | 168 | 112 | 6 | 25.0 | 527.4 | 205 | 3.5 | 25.2 | 3.0 | 20.8 |
| F1-0.5-30 | 30 | 175 | 116 | 6 | 10.0 | 590.3 | 198 | 0.5 | 26.6 | 3.0 | 20.3 |
| F2-1.1-30 | | 174 | 117 | 8 | 12.5 | 590.3 | 196 | 1.1 | 26.9 | 3.1 | 20.5 |
| F3-2.2-30 | | 170 | 115 | 6 | 20.0 | 506.7 | 190 | 2.2 | 26.9 | 3.1 | 20.5 |
| F4-3.5-30 | | 168 | 117 | 6 | 25.0 | 527.4 | 205 | 3.5 | 26.6 | 3.0 | 20.3 |
| F1-0.5-100 | 100 | 175 | 116 | 6 | 10.0 | 590.3 | 198 | 0.5 | 27.2 | 2.7 | 17.4 |
| F2-1.1-100 | | 174 | 113 | 8 | 12.5 | 590.3 | 196 | 1.1 | 25.3 | 2.7 | 16.7 |
| F3-2.2-100 | | 170 | 118 | 6 | 20.0 | 506.7 | 190 | 2.2 | 25.3 | 2.7 | 16.7 |
| F4-3.5-100 | | 168 | 112 | 6 | 25.0 | 527.4 | 205 | 3.5 | 27.2 | 2.7 | 17.4 |

Note: $d_s$ = 16 mm; $d_h$ = 50 mm.

### *3.4. Instrumentation, Monitoring, and Testing System*

Three vertical displacement transducers (linear variable differential transformer—LVDT) were installed in different places to determine the displacements. The transducer arrangement is shown in Figure 4. LVDT 1 was positioned on the side of the prism to measure the vertical displacements caused by the bending of the specimen at the time of the test. LVDT 2 was aligned with the headed bar on the underside of the specimen to monitor the slippage of the head. The third device (LVDT 3) was positioned near the headed bar's shank on the specimen's upper surface within the concrete cone region. The

positioning of the transducers enabled monitoring of the prism deflection and headed bars' slippage in the concrete during the test.

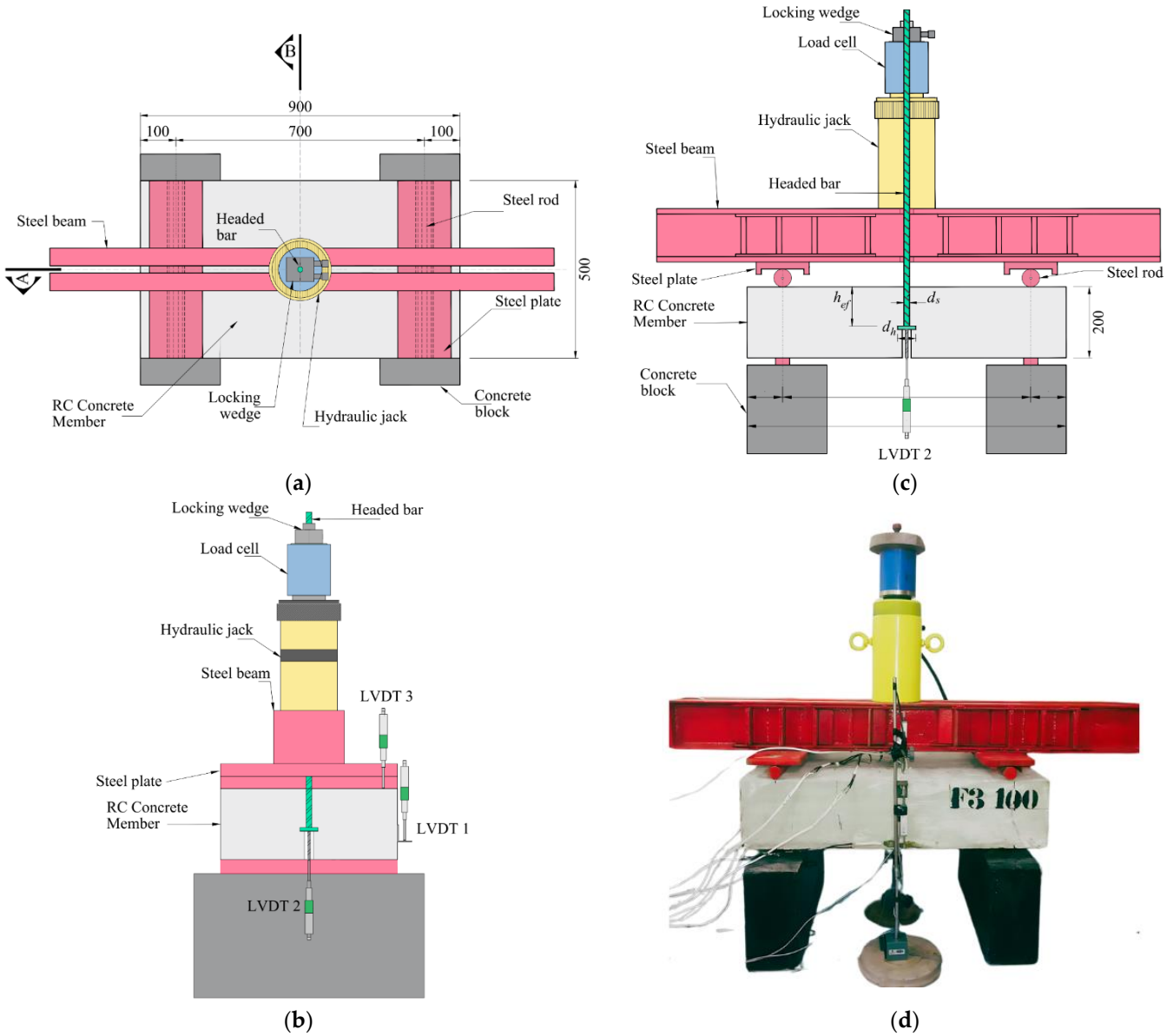



**Figure 4.** Test setup: (**a**) plain view, (**b**) Section B-B, (**c**) Section A-A, and (**d**) setup test picture.

The strains in the flexural reinforcement were monitored by two strain gauges, *ef*1 and *ef*2. The devices were positioned in the longitudinal direction of the reinforcements, in the middle of the total length of the bending bar, and located in the bar closest to the head of the connector (see Figure 5).

The area of the concrete cone was monitored by four immersion strain gauges positioned perpendicular to the plane of formation of the theoretical crack of the concrete cone, which occurs at 35° inclination in relation to the bars' head, according to ACI 318 [12]. The cross-section and the longitudinal section of the prisms were monitored by two strain gauges each, one positioned near the head of the connector (CLB and CTB) and another near the flexural reinforcements (CLA and CTA) (see Figure 5).

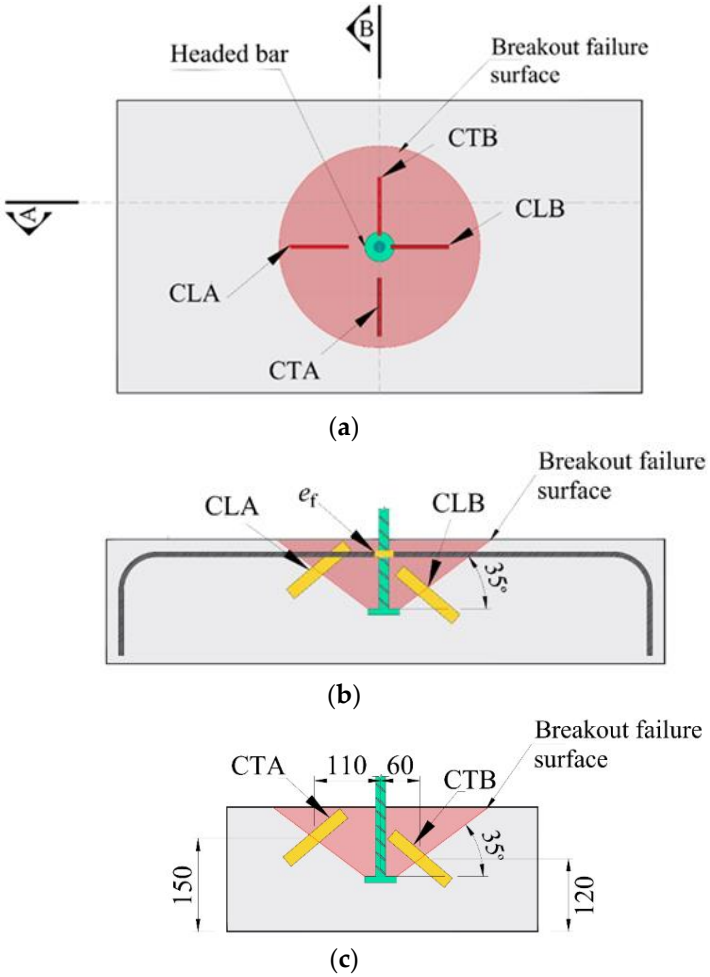



**Figure 5.** Details of the instrumentation with embedded strain gauges: (**a**) plain view, (**b**) Section A-A, and (**c**) Section B.

During the test, the upper surface of the prism was observed until the first flexural crack appeared. This crack was monitored using a crack comparator, and the variation in its width was recorded as a function of the increase in the load. Only one crack in each prism was monitored during the entire test until the concrete breakout.

The infrastructure for conducting the tests is shown in Figure 4, including two concrete blocks, two steel rollers to support the specimens, and a steel hollow reaction beam. Two steel sheets were fixed to the reaction beam to simulate type 1 and 2 supports. The load application system consisted of a hydraulic hollow cylinder driven by a hydraulic pump, and the load was applied continuously. The load reading was performed through a load cell connected to a data acquisition system (DAS). The hydraulic cylinder and load cell assembly were positioned above the reaction beam and anchored to the shank of the headed bar through a wedging system.

## 4. Results and Discussion

### *4.1. Effect of RCA and ρf % on Vertical Displacement*

The load–displacement behavior of the prisms per test series is shown in Figure 6. As expected, the increase in the flexural reinforcement ratio altered the vertical displacement of the tested specimens.

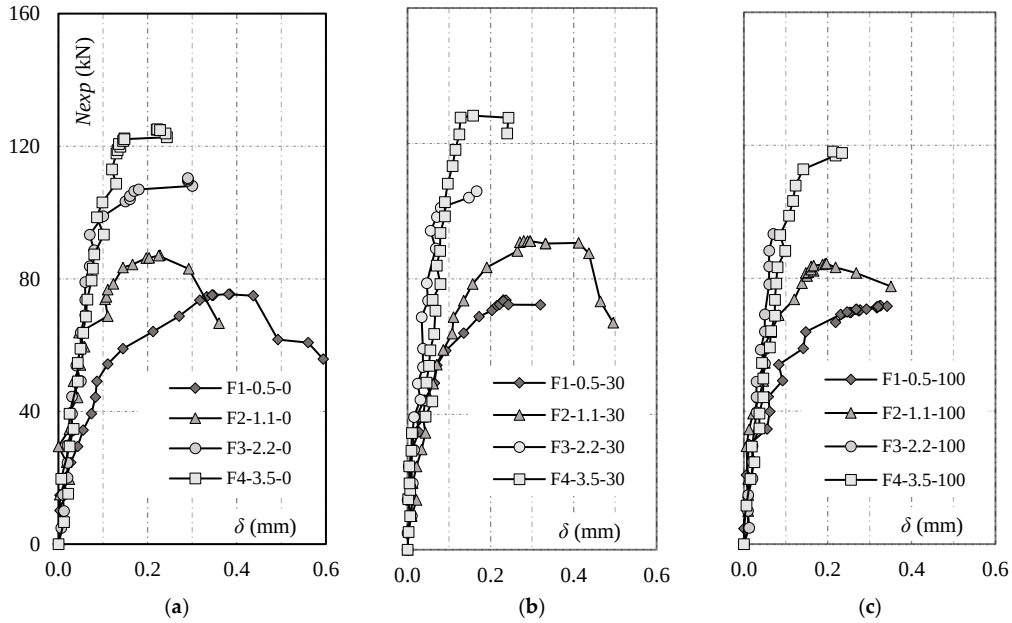



**Figure 6.** Load–displacement curves as a function of the flexural reinforcement ratio: (**a**) 0% of RCA, (**b**) 30% of RCA, and (**c**) 100% of RCA.

To verify the effect of RCA addition on the load–displacement response, the overlapping curves of specimens with the same flexural reinforcement ratio and different percentages of recycled aggregate were plotted (see Figure 6). In general, RCA addition did not affect the load–displacement behavior of the specimens. The interaction mechanism between the flexural reinforcement and the concrete acted similarly and did not depend on the amount of RCA for the case studied.

### *4.2. Strains in the Flexural Reinforcement*

The strains measured in the flexural reinforcement bars are shown in Figure 7. Analysis of the load–strain curves indicates that the steel was in the elastic regime.

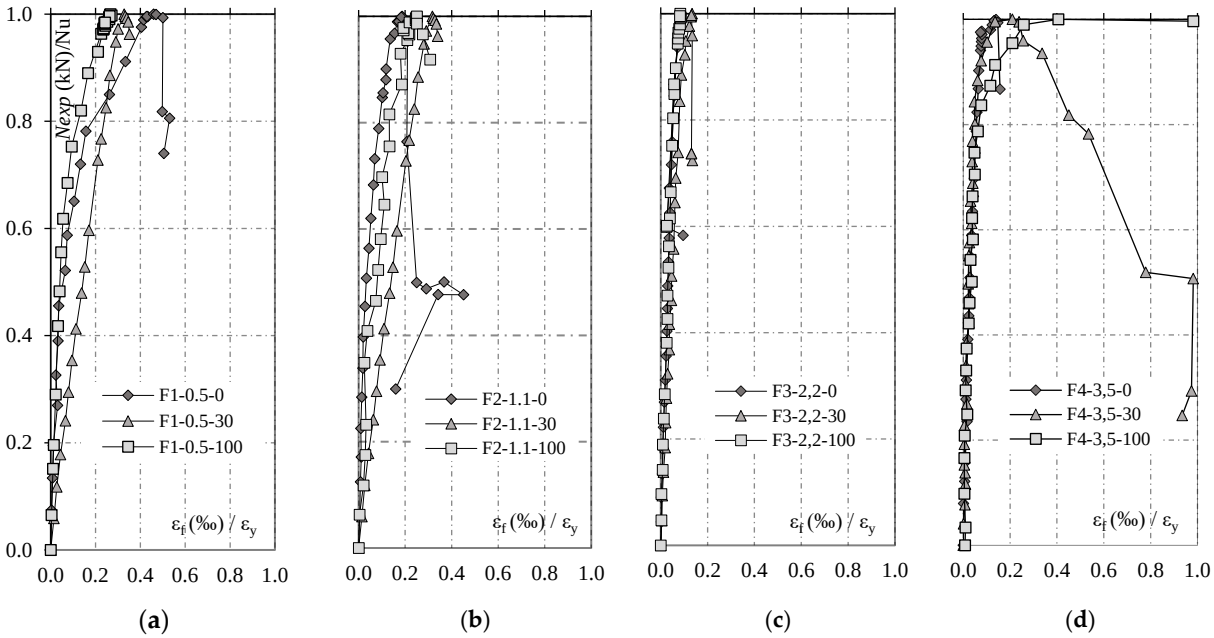



**Figure 7.** Strains in the flexural reinforcement: (**a**) $\rho f$ = 0.5%, (**b**) $\rho f$ = 1.1%, (**c**) $\rho f$ = 2.2%, and (**d**) ρf = 3.5%.

In the design of the prisms, the dimensions were set to ensure that the section could withstand the flexural stresses caused by the tensile force applied to the headed bar. Thus, as shown in Figure 7, no strains were recorded that would constitute steel yielding and consequent flexural failure. The graphs also show that the rebars reached the same strain level up to approximately 40 kN, which is approximately the crack load of the tested specimens. The largest strains were recorded in the reinforcements of the F1-0.5-type prisms. The higher level of the strains in the rebars indicates that the specimen was in a greater state of cracking, which explains the lower load capacity of the less reinforced prisms.

### *4.3. Effect of RCA and ρf on Crack Width*

The crack width monitoring results according to the load application of the tested series are shown in Figure 8. The readings were taken manually with a crack comparator, and after the appearance of the first visual flexural crack in the specimen, readings were recorded at each 5 kN load step. The results indicate that the increase in the flexural reinforcement ratio affected the crack width in the prisms, and the crack control exerted by the steel promoted a greater load capacity in the concrete–anchor connection. Figure 8 presents the load–crack width curve for specimens with the different flexural reinforcement ratio and different substitution percentages. As shown in this figure, the increase in the RCA amount did not alter the cracking pattern

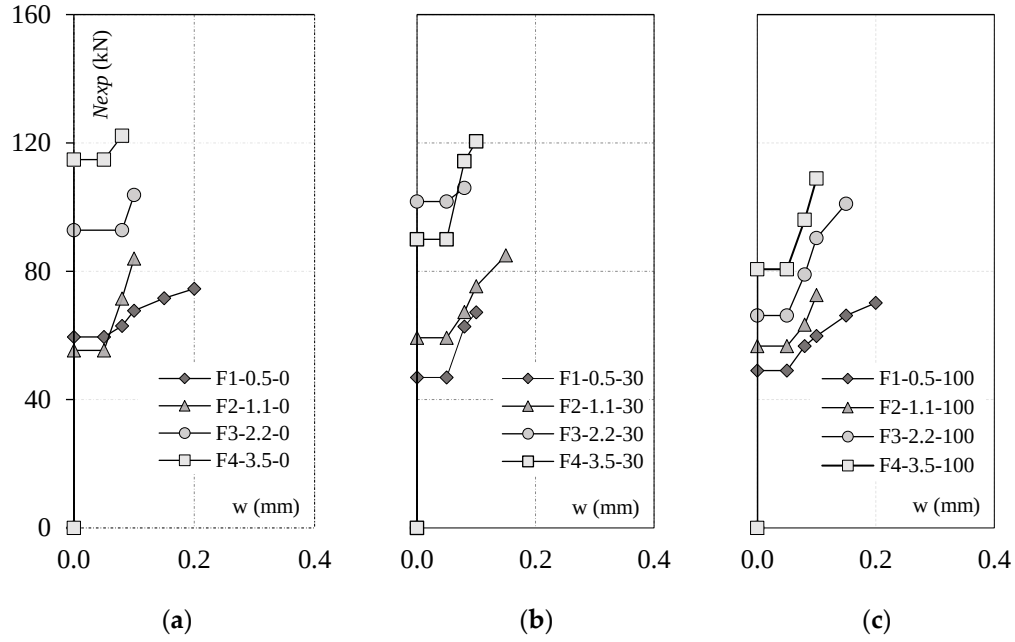



**Figure 8.** Load–crack widths as a function of the flexural reinforcement ratio: (**a**) 0% of RCA, (**b**) 30% of RCA, and (**c**) 100% of RCA.

Figure 9 presents the load–crack width curve for specimens with the same flexural reinforcement ratio for different percentages of natural aggregate substitution. As shown in this figure, using RCA had a small impact on the tested specimens' crack width.

Figure 10 illustrates the relationship between $k_{exp}$ and the theoretical crack width (wk) calculated based on the recommendations presented by MC10 [41]. This figure includes data from tests conducted by Takiguichi, K. et al. [42], Eligehausen, R. and Ozbolt, J. [37], Ferreira, M et al. [16], Santana, P.F [17], and Yoon, Y. S et al. [43], along with the results originally presented in this paper. It is noteworthy that crack widths substantially impact the concrete breakout strength of the headed anchors. The larger the crack widths, the lower the concrete breakout strength, showing that controlling cracks can ensure a greater load-carrying capacity for the headed anchors. Furthermore, Figure 10 also shows that the

concrete breakout strength of the tested specimens with 30% and up to 100% of RCA was similar to the resistance of specimens with natural coarse aggregates.

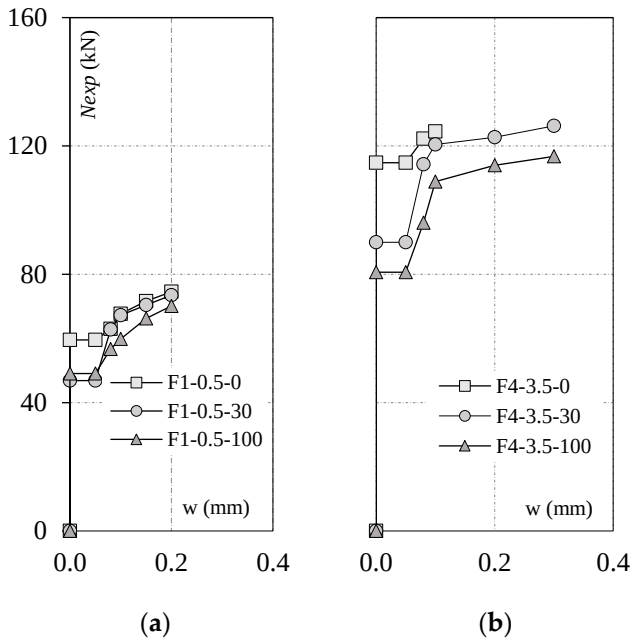



**Figure 9.** Load–crack widths as a function of the percentage of RCA: (**a**) ρf = 0.5% and (**b**) ρf = 3.5%.

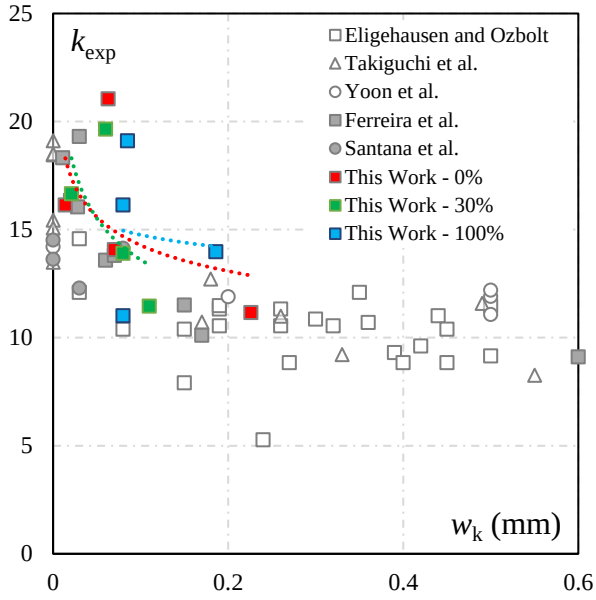



**Figure 10.** Variation in $k_{exp}$ as a function of the theoretical crack width, Takiguichi, K. et al. [42], Eligehausen, R. and Ozbolt, J. [37], Ferreira, M et al. [16], Santana, P.F [17], and Yoon, Y. S et al. [43]).

### *4.4. Slippage of the Headed Bar*

These results investigate the slippage of the headed bars, which may occur due to failure in the anchoring system, as reported by Eligehausen, R [14]. The displacement as a function of the load is shown in Figure 11. Plotting the graphs according to the test series revealed that the flexural reinforcement ratio affected the slippage of the head, while the concrete cracking level decreased as a function of the increase in the steel area of the specimen. In addition, the displacement of the headed bar remained low until the load was close to the concrete breakout resistance, and larger displacements were recorded only after

the ultimate load when the concrete cone was observed. These results show that there was no anchorage failure in any of the tested specimens.

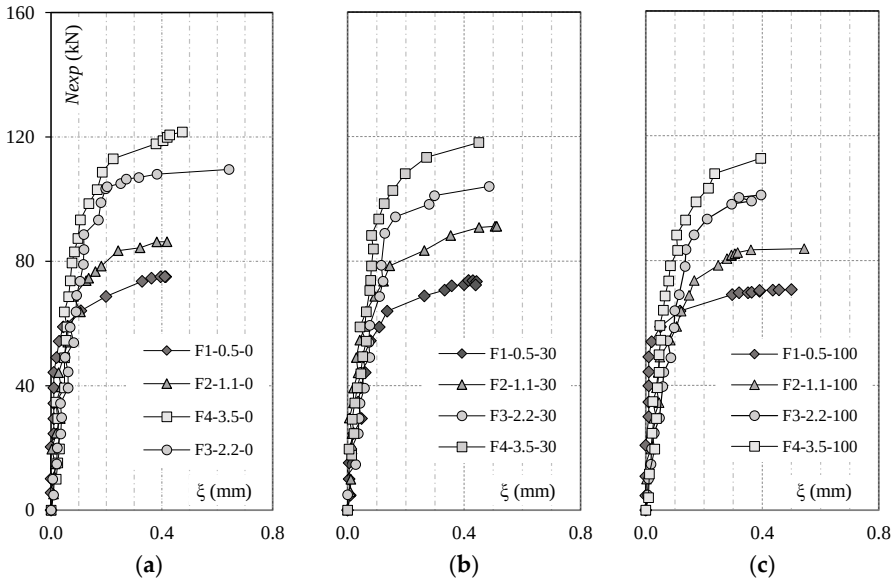



**Figure 11.** Load–slip curves of the headed bars as a function of the flexural reinforcement ratio: (**a**) 0% of RCA, (**b**) 30% of RCA, and (**c**) 100% of RCA.

When the anchoring system is guaranteed, according to Eligehausen, R [14], small slippages of the headed bar occur when the concrete area adhered to the embedded length of the bar begins to crack due to the stresses arising from the application of the localized load exerted by the head of the anchor, which can cause crushing of the concrete. Figure 12 compares the slippage measured in the headed bar for specimens with the same flexural reinforcement ratio and RCA percentages. The slippage response was not affected by using recycled concrete aggregates, which indicates that the anchor–concrete interaction did not depend on the RCA substitution content in this case.

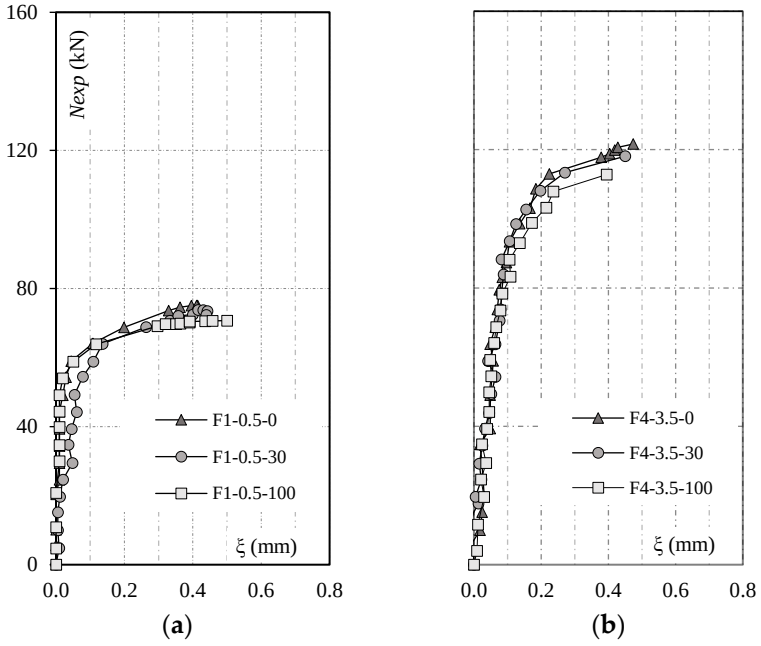



**Figure 12.** Load–slip curves of the headed bars as a function of the percentage of RCA: (**a**) ρf = 0.5% and (**b**) ρf = 3.5%.

### *4.5. Effect of RCA on Strains in the Concrete Cone*

The strains recorded in the concrete cone are shown in Figure 13. The monitoring results show that the strains near the head of the headed bar were greater, while the concrete portion near the flexural reinforcement presented smaller strain values. This pattern shows that the area surrounding the head of the bar was the first to undergo microcracking because this is where the cracking of the concrete cone crack originated, according to Eligehausen, R. and Sawade, G. [35]. This region relies only on concrete to absorb tensile forces, and due to the low strength of the material to this type of stress, the region ends up undergoing greater strains. The behavior recorded in the reference series was also observed in specimens with 30% and 100% substitution. Even with some variations, the response pattern of the strain of the concrete cone was generally maintained, which indicates that the strains of the concrete cone were not affected by increases in the recycled aggregate content.

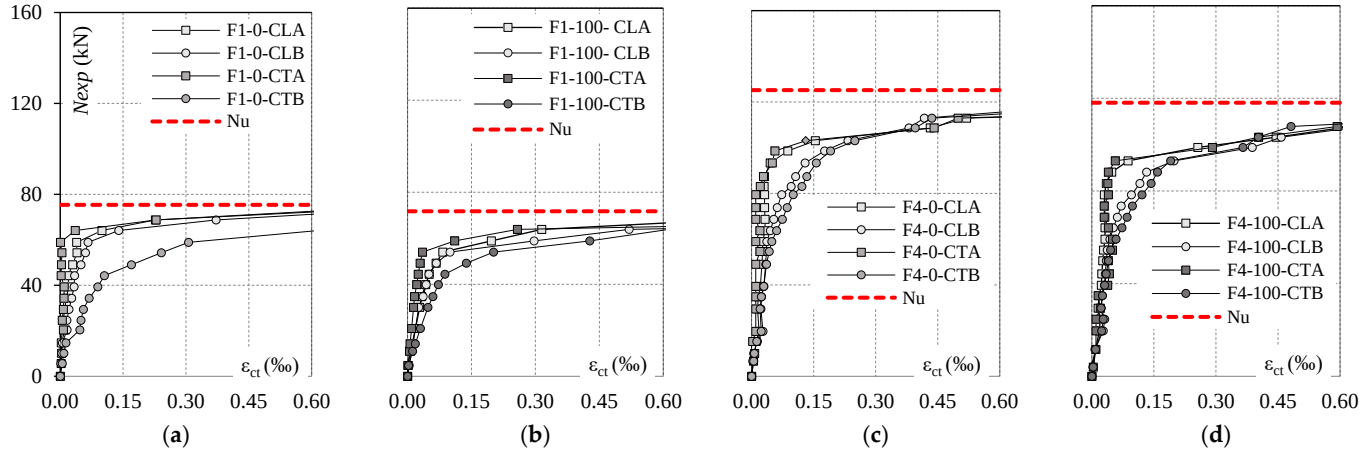



**Figure 13.** Strains within the concrete cone: (**a**) ρf = 0.5% and 0% of RCA, (**b**) ρf = 0.5% and 100% of RCA, (**c**) $\rho_f$ = 3.5% and 0% of RCA, and (**d**) ρf = 3.5% and 100% of RCA.

Figure 14 shows the variation in transverse strains in concrete within the projection of the failure cone at different load stages. It is possible to observe that the tensile strains in concrete develop stably in the failure projection and that up to 60% Nu, the strains were smaller than the tensile fracture strain of the concrete, typically 0.15‰. The results show that the critical crack initiates at the anchor head and spreads stably toward the concrete surface, as described by 35. Eligehausen, R. and Sawade, G. [35]. Figure 15 presents the strains in concrete for specimens with 0% and 100% replacement of natural aggregates with recycled concrete aggregates. It is observable that the utilization of RCA does not significantly impact the tensile strains within the concrete failure cone.

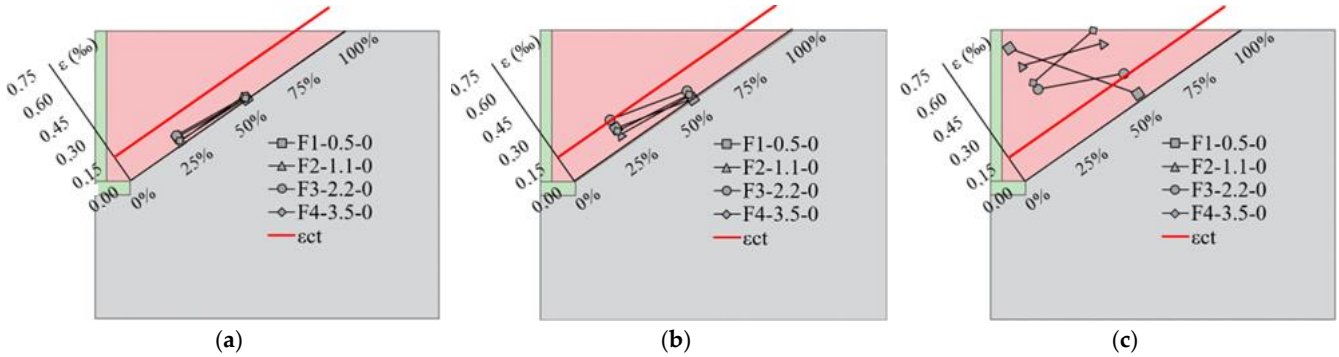



**Figure 14.** Strains in concrete for different load stages: (**a**) 30% $N_u$, (**b**) 60% $N_u$, and (**c**) 90% $N_u$.

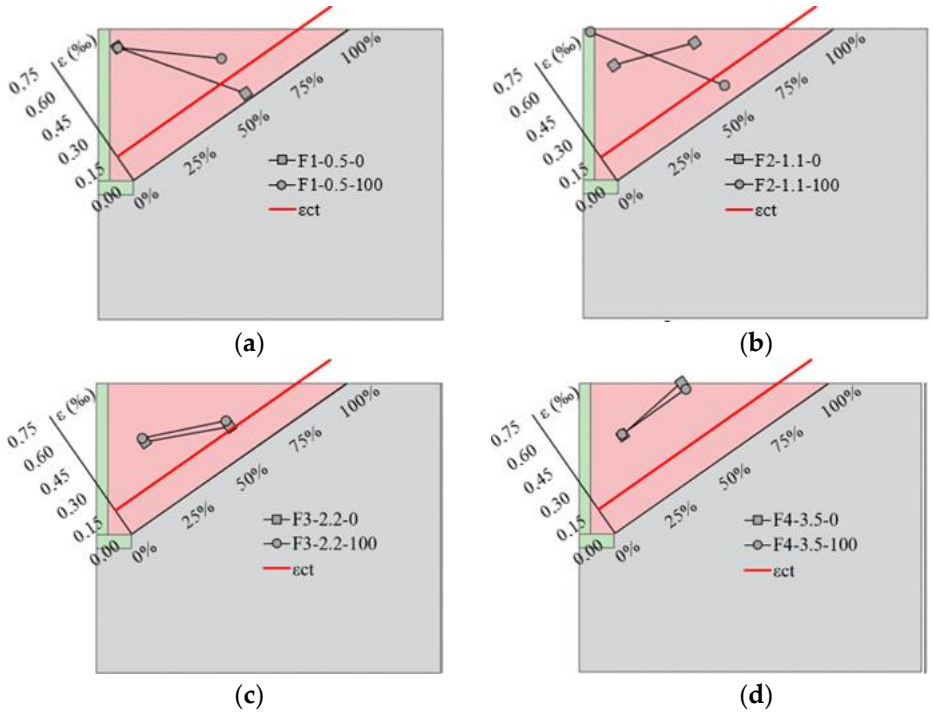



**Figure 15.** Strains in concrete for different percentages of RCA: (**a**) specimen F1, (**b**) specimen F2, (**c**) specimen F3, and (**d**) specimen F4.

### *4.6. Effect of RCA in the Concrete Breakout Strength and Failure Modes*

Figure 16 shows photos of the specimens with 0% RCA and 100% RAC after failure. Side and top photos of the specimens after testing are shown. All specimens showed concrete cone failure.

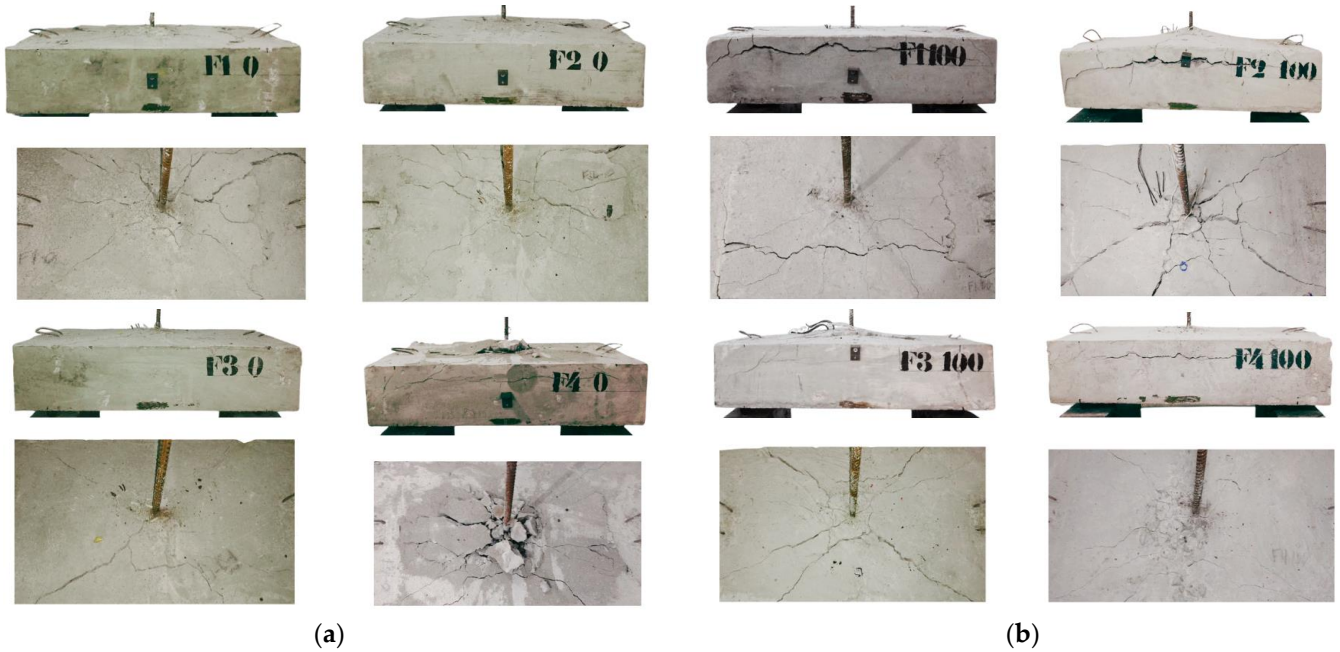



**Figure 16.** Photos of the tested specimens after failure: (**a**) 0% RCA and (**b**) 100% RCA.

Initially, the failure was characterized by cracks parallel to the flexural reinforcements on the surface of the concrete specimens, which spread through their breadths towards the edges. The tangential cracks resulting from the formation of the concrete failure cone were

observed concomitantly with the ultimate load. The tested specimens did not present signs of flexural, shear, or any other types of failure modes.

Table 5 compares the tested specimens' experimental and theoretical concrete breakout resistance. In addition, to evaluate the performance of the theoretical predictions in relation to the experimental result, the parameter λ was plotted for each design code. λ expresses the relationship between the experimental and the theoretical resistances.

**Table 5.** Summary of experimental and theoretical results.

| Specimen | % of RCA | $h_{ef}$ mm | $\rho_f$ % | $N_{exp}$ (kN) | $\lambda_{fib}$ | $\lambda_{ACI}$ |
|---|---|---|---|---|---|---|
| F1-0.5-0 | 0 | 119 | 0.5 | 75.4 | 1.25 | 1.12 |
| F2-1.1-0 | | 115 | 1.1 | 87.1 | 1.58 | 1.41 |
| F3-2.2-0 | | 120 | 2.2 | 110.4 | 1.81 | 1.61 |
| F4-3.5-0 | | 112 | 3.5 | 125.2 | 2.36 | 2.10 |
| F1-0.5-30 | 30 | 116 | 0.5 | 73.8 | 1.29 | 1.14 |
| F2-1.1-30 | | 117 | 1.1 | 91.2 | 1.56 | 1.39 |
| F3-2.2-30 | | 115 | 2.2 | 106.5 | 1.87 | 1.66 |
| F4-3.5-30 | | 117 | 3.5 | 128.2 | 2.21 | 1.96 |
| F1-0.5-100 | 100 | 116 | 0.5 | 71.7 | 1.24 | 1.10 |
| F2-1.1-100 | | 113 | 1.1 | 84.4 | 1.57 | 1.40 |
| F3-2.2-100 | | 118 | 2.2 | 104.0 | 1.81 | 1.61 |
| F4-3.5-100 | | 112 | 3.5 | 118.1 | 2.15 | 1.91 |

After tests, it was observed that the variation in some parameters could affect the experimental concrete breakout strength. To evaluate the experimental results, Equation (2) was used to calculate the experimental value of factor *k*.

$$k_{Exp} = \frac{N_{Exp}}{\sqrt{fc} \cdot h_{ef}^{0.5}} \quad (2)$$

In general, the strength estimates consider the concrete's tensile strength and the headed bar's effective embedment. Currently, no normative prescription considers the flexural reinforcement ratio of the structural elements, in which headed anchors are used as a portion of the concrete breakout strength of the anchor. In this context, the design code models are constant and consider only the cracking state of concrete.

Figure 17 shows the flexural reinforcement ratio as a function of the parameter $k_{Exp}$. In addition, the limiting values presented by [12,13] were also plotted for the cracked and uncracked concrete conditions. Based on this figure, the flexural reinforcement ratio significantly affects $k_{Exp}$, whereas the limiting value provided by the standards becomes over-conservative as the flexural reinforcement ratio increases. Thus, it is pertinent to indicate that the concrete breakout strength of headed anchors is not only related to the mechanical properties of the concrete or the effective embedment of the connector but can also be linked to the flexural resistance of the structural member, as the flexural reinforcement control the cracking state of concrete.

The experimental results presented in this article are compared with those presented by Ferreira, M et al. [16] and Nilsson, M et al. [15] (see Figure 18). As shown in Figures 18 and 19, recycled concrete aggregates did not change the concrete breakout strength of the headed bars. Furthermore, it is shown that the flexural reinforcement ratio influences the concrete breakout resistance, irrespective of the use of recycled concrete aggregates. Assuming that concrete is cracked, Figure 18 also compares the k-factor values established by fib and ACI. The design code values become over-conservative with increments of the flexural reinforcement ratio.

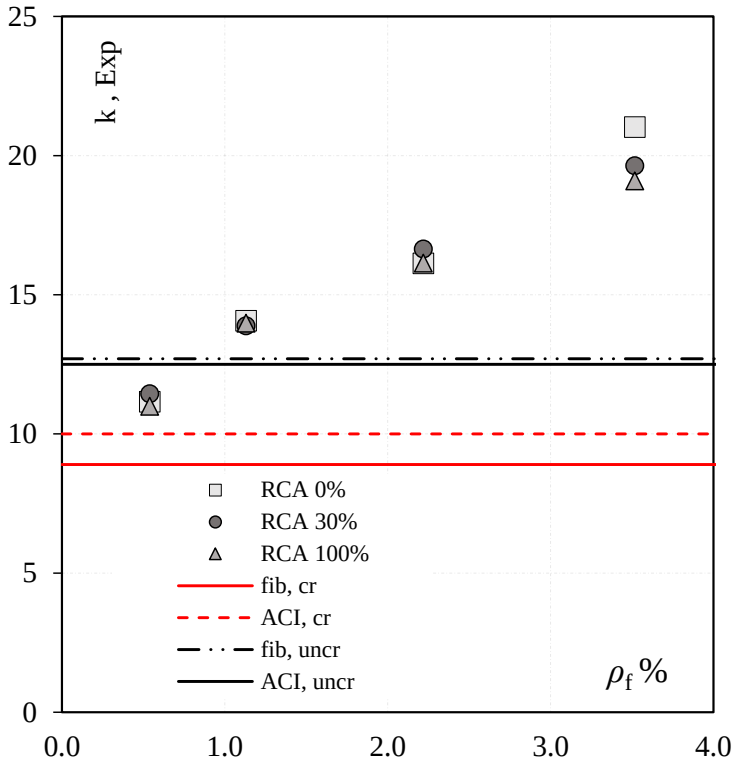



**Figure 17.** Variation in $k_{Exp}$ as a function of the flexural reinforcement ratio.

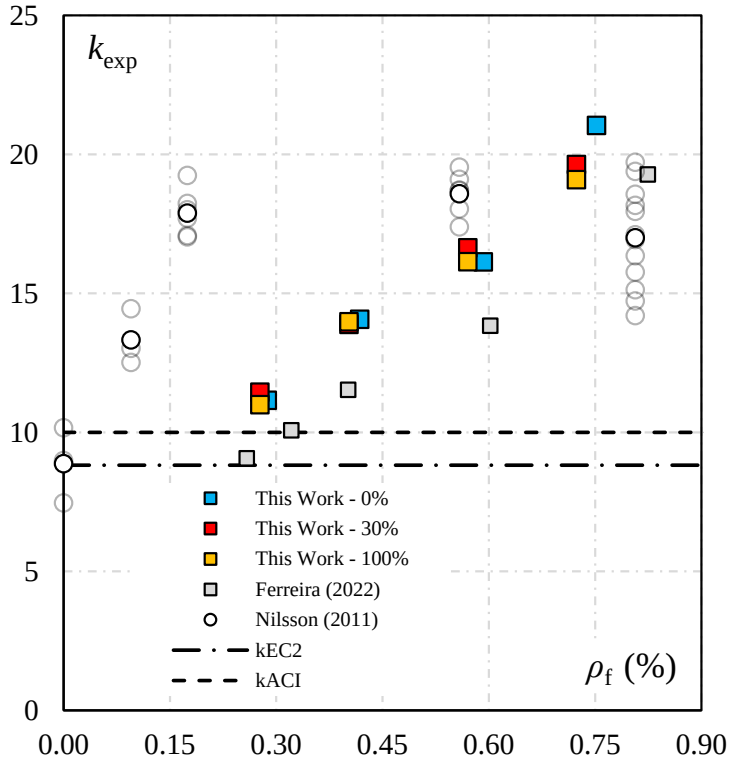



**Figure 18.** Variation in $k_{Exp}$ as a function of the flexural reinforcement ratio considering results from the literature, Ferreira, M et al. [16] and Nilsson, M et al. [15]).

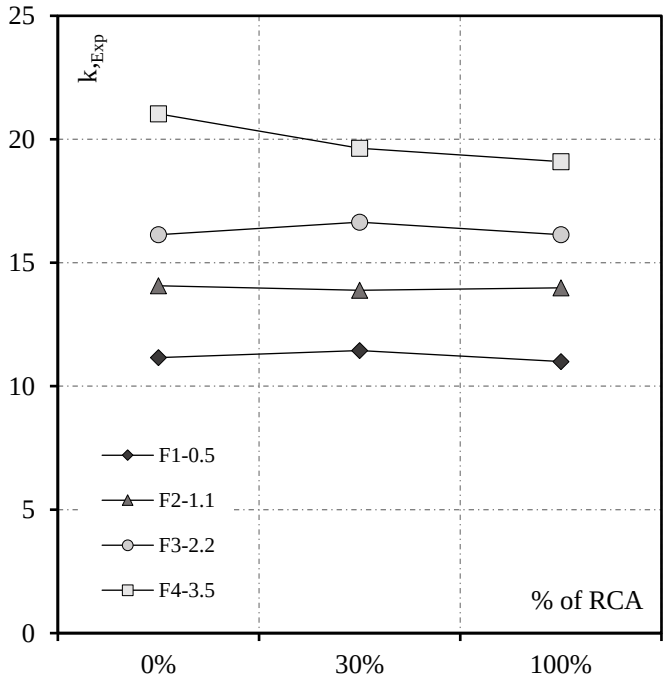



**Figure 19.** Variation in the factor $k_{Exp}$ as a function of the percentage of RCA.

## 5. Conclusions

- Using RCA did not affect the response of headed bars embedded in slender reinforced concrete structural members. On the other hand, increments of the flexural reinforcement ratio significantly affected the response and the concrete breakout strength of the headed bars due to the reduction in crack widths before failure.
- Measuring the internal strains in the projection of the concrete failure cone indicates that the critical crack starts at the anchor's head and extends towards the concrete surface. Furthermore, increasing the flexural reinforcement ratio controls the crack widths, thus increasing the concrete breakout resistance of the tested headed bars. Furthermore, using RCA did not affect the strains of the concrete cone, regardless of the aggregate replacement percentage.
- The concrete breakout strength of the tested headed bars was related not only to the mechanical properties of the concrete and the effective embedment of the anchor but also to the flexural reinforcement ratio of the specimens, regardless of the substitution of natural coarse aggregates by recycled concrete aggregates.
- In terms of the design code approaches (see [12,13]), the theoretical estimates become over-conservative as the flexural reinforcement ratio increases, evidencing that this is a parameter that should be taken into account in cases of headed bars embedded in slender structural members.
- Using recycled concrete aggregates instead of natural coarse aggregates did not affect the concrete breakout strength of headed bars embedded in slender structural members. These findings indicate that utilizing RCA for structural applications in the precast concrete industry is a feasible alternative, but further scientific research is needed.

**Author Contributions:** Conceptualization, M.d.P.F. and K.D.d.S.; Methodology, M.d.P.F. and K.D.d.S.; Formal analysis, K.D.d.S.; Writing—original draft, M.d.P.F. and K.D.d.S.; Writing—review & editing, M.d.P.F. and M.J.M.P.F.; Supervision, L.d.N.P.C. All authors have read and agreed to the published version of the manuscript.

**Funding:** The authors received no financial support for the research but received financial support for the publication of this article from PROPESP/PAPQ/UFPA.

**Data Availability Statement:** Data are contained within the article.

**Conflicts of Interest:** The authors declare no conflict of interest.

## Abbreviations

| | |
|---|---|
| RCA | coarse recycled concrete aggregate |
| NCA | natural coarse aggregate |
| NQS | natural quartz sand |
| m | unit mass |
| p | unit proportion of fine aggregates |
| pRCA | proportion of coarse recycled concrete aggregate |
| W/C | water–cement ration |
| C | cement consumption |
| d | effective depth of specimen |
| ds | diameter of the anchor shank |
| dh | diameter of the anchor head |
| fc | concrete compressive strength |
| fct | concrete tensile strength |
| h | height of the concrete specimen |
| hef | embedment depth |
| *ef* | strain gauge that monitors the flexural reinforcement |
| CLA | strain gauge that monitors the concrete longitudinally near the head of the connector |
| CLB | strain gauge that monitors the concrete longitudinally near the flexural reinforcement |
| CTA | strain gauge that monitors the concrete cross-section near the head of the connector |
| CTB | strain gauge that monitors the concrete cross-section near the flexural reinforcement |
| LVDT | linear variable differential transformer |
| k | coefficient to account for the influence of the cracking state of the concrete in the concrete cone resistance |
| kexp | coefficient measured on tests, calculated as Nu/(fc0.5 · hef1.5) |
| kuncr | coefficient to consider that the anchor was placed on an uncracked concrete zone |
| nf | number of flexural rebars in the tested specimen |
| wk | concrete crack width |
| Eci | modulus of elasticity of the concrete |
| Ef | modulus of elasticity of the flexural reinforcement |
| Nu | tensile strength of an anchor for concrete cone failure |
| Nexp | experimental strength of the specimens |
| δ | displacement of the flexural reinforcement |
| εct | strain on the concrete surface |
| εf | strain on reinforcement steel |
| εy | yield strain of reinforcement steel |
| Øf | diameter of the flexural reinforcement |
| ξ | slip of the headed bars |
| ρf | flexural reinforcement ratio |

## References

1. Omary, S.; Ghorbel, E.; Wardeh, G. Relationships between recycled concrete aggregates characteristics and recycled aggregates concretes properties. *Constr. Build. Mater.* **2016**, *108*, 163–174. [CrossRef]
2. Koper, A.; Koper, W.; Koper, M. Influence of Raw Concrete Material Quality on Selected Properties of Recycled Concrete Aggregates. *Procedia Eng.* **2017**, *172*, 536–543. [CrossRef]
3. Pedro, D.; De Brito, J.; Evangelista, L. Mechanical characterization of high performance concrete prepared with recycled aggregates and silica fume from precast industry. *J. Clean. Prod.* **2017**, *164*, 939–949. [CrossRef]
4. Salesa, Á.; Pérez-Benedicto, J.Á.; Esteban, L.M.; Vicente-Vas, R.; Orna-Carmona, M. Physico-mechanical properties of multi-recycled self-compacting concrete prepared with precast concrete rejects. *Constr. Build. Mater.* **2017**, *153*, 364–373. [CrossRef]
5. Fiol, F.; Thomas, C.; Muñoz, C.; Ortega-López, V.; Manso, J.M. The influence of recycled aggregates from precast elements on the mechanical properties of structural self-compacting concrete. *Constr. Build. Mater.* **2018**, *182*, 309–323. [CrossRef]
6. Bai, G.; Zhu, C.; Liu, C.; Liu, B. An evaluation of the recycled aggregate characteristics and the recycled aggregate concrete mechanical properties. *Constr. Build. Mater.* **2020**, *240*, 117978. [CrossRef]

7. Berredjem, L.; Arabi, N.; Molez, L. Mechanical and durability properties of concrete based on recycled coarse and fine aggregates produced from demolished concrete. *Constr. Build. Mater.* **2020**, *246*, 118421. [CrossRef]
8. Seara-Paz, S.; González-Fonteboa, B.; Martínez-Abella, F.; Eiras-López, J. Flexural performance of reinforced concrete beams made with recycled concrete coarse aggregate. *Eng. Struct.* **2018**, *156*, 32–45. [CrossRef]
9. Huang, Y.; Xiao, J.; Zhang, C. Theoretical study on mechanical behavior of steel confined recycled aggregate concrete. *J. Constr. Steel Res.* **2012**, *76*, 100–111. [CrossRef]
10. Katkhuda, H.; Shatarat, N. Shear behavior of reinforced concrete beams using treated recycled concrete aggregate. *Constr. Build. Mater.* **2016**, *125*, 63–71. [CrossRef]
11. Malešev, M.; Radonjanin, V.; Marinković, S. Recycled concrete as aggregate for structural concrete production. *Sustainability* **2010**, *2*, 1204–1225. [CrossRef]
12. *ACI Committee 318*; Building Code Requirements for Structural Concrete (ACI 318-19). ACI: Farmington Hills, MI, USA, 2019.
13. Fédération Internationale du Béton. *FIB Bulletin 58—Design of Anchorage in Concrete*; FIB: Lausanne, Switzerland, 2011.
14. Eligehausen, R.; Mallée, R.; Silva, J. *Anchorage in Concrete Construction*, 1st ed.; Ernst & Sohn GmbH & Co.: Hoboken, NJ, USA, 2006.
15. Nilsson, M.; Ohlsson, U.; Elfgren, L. Effects of surface reinforcement on bearing capacity of concrete with anchor bolts. *Cem. Concr. Res.* **2018**, *44*, 161–174.
16. Ferreira, M.; Filho, M.P.; Lima, N.; Oliveira, M. Influence of the flexural and shear reinforcement in the concrete cone resistance of headed bars. *Eng. Struct.* **2021**, *248*, 113212. [CrossRef]
17. Santana, P.F.; Silva, P.C.; Ferreira, M.P.; Bezerra, L.M.; Oliveira, M.H. Experimental and numerical study of headed bars embedded in RC members under tension. *Struct. Eng. Mech.* **2022**, *84*, 531–546. [CrossRef]
18. Elsayed, M.; Abd-Allah, S.R.; Said, M.; El-Azim, A.A. Structural performance of recycled coarse aggregate concrete beams containing waste glass powder and waste aluminum fibers. *Case Stud. Constr. Mater.* **2023**, *18*, e01751. [CrossRef]
19. Rahal, K.; Alrefaei, Y. Shear strength of longitudinally reinforced recycled aggregate concrete beams. *Eng. Struct.* **2017**, *145*, 273–282. [CrossRef]
20. McNeil, K.; Kang, T.H.-K. Recycled Concrete Aggregates: A Review. *Int. J. Concr. Struct. Mater.* **2013**, *7*, 61–69. [CrossRef]
21. Akbarnezhad, A.; Ong, K.C.G. Separation processes to improve the quality of recycled concrete aggregates (RCA). In *Handbook of Recycled Concrete and Demolition Waste*; Elsevier Inc.: Amsterdam, The Netherlands, 2013; pp. 246–269. [CrossRef]
22. Saravanakumar, P.; Abhiram, K.; Manoj, B. Properties of treated recycled aggregates and its influence on concrete strength characteristics. *Constr. Build. Mater.* **2016**, *111*, 611–617. [CrossRef]
23. Kubissa, W.; Jaskulski, R.; Koper, A.; Szpetulski, J. Properties of concretes with natural aggregate improved by RCA addition. *Procedia Eng.* **2015**, *108*, 30–38. [CrossRef]
24. Behera, M.; Bhattacharyya, S.; Minocha, A.; Deoliya, R.; Maiti, S. Recycled aggregate from C&D waste & its use in concrete—A breakthrough towards sustainability in construction sector: A review. *Constr. Build. Mater.* **2014**, *68*, 501–516. [CrossRef]
25. Hansen, T.C. Recycled aggregate and recycled aggregate concrete, second state of- the-art report, developments from 1945–1985. *Mater. Struct.* **1986**, *19*, 201–246. [CrossRef]
26. Casuccio, M.; Torrijos, M.; Giaccio, G.; Zerbino, R. Failure mechanism of recycled aggregate concrete. *Constr. Build. Mater.* **2008**, *22*, 1500–1506. [CrossRef]
27. Padmini, A.K.; Ramamurthy, K.; Mathews, M.S. Influence of parent concrete on the properties of recycled aggregate concrete. *Constr. Build. Mater.* **2009**, *23*, 829–836. [CrossRef]
28. Cabral, A.E.B.; Schalch, V.; Molin, D.C.C.D.; Ribeiro, J.L.D. Mechanical properties modeling of recycled aggregate concrete. *Constr. Build. Mater.* **2010**, *24*, 421–430. [CrossRef]
29. Paine, K.; Dhir, R. Recycled aggregates in concrete: A performance-related approach. *Mag. Concr. Res.* **2010**, *62*, 519–530. [CrossRef]
30. Limbachiya, M.C.; Leelawat, T.; Dhir, R.K. Use of recycled concrete aggregate in high-strength concrete. *Mater. Struct.* **2000**, *33*, 574–580. [CrossRef]
31. Çakir, O. Experimental analysis of properties of recycled coarse aggregate (RCA) concrete with mineral additives. *Constr. Build. Mater.* **2014**, *68*, 17–25. [CrossRef]
32. Silva, R.; de Brito, J.; Dhir, R. Tensile strength behaviour of recycled aggregate concrete. *Constr. Build. Mater.* **2015**, *83*, 108–118. [CrossRef]
33. Xiao, J.; Li, J.; Zhang, C. Mechanical properties of recycled aggregate concrete under uniaxial loading. *Cem. Concr. Res.* **2005**, *35*, 1187–1194. [CrossRef]
34. Gomes, M.; de Brito, J. Structural concrete with incorporation of coarse recycled concrete and ceramic aggregates: Durability performance. *Mater. Struct.* **2009**, *42*, 663–675. [CrossRef]
35. Eligehausen, R.; Sawade, G. *A Fracture Mechanics Based Description of the Pull-Out Behavior of Headed Studs Embedded in Concrete, Elfgren, Lennart (Hrsg.): Fracture Mechanics of Concrete Structures*; Chapman and Hall: London, UK, 1989; pp. 281–299. ISBN 0-412-30680-8.
36. Eligehausen, R. Behavior, Design and Testing of Anchors in Cracked Concrete. *ACI Struct. J.* **1992**, *130*, 123–176.

37. Ozbolt, J.; Eligehausen, R. Numerical Analysis of Headed Studs embedded in Large Plain Concrete Blocks. In Proceedings of the 2nd International Conference of Computer Aided Analysis and Design of Concrete Structures, Zell am See, Austria, 4–6 April 1990.
38. Di Nunzio, G.; Muciaccia, G. Cast-in-place fasteners under tensile loading: A critical review. *Structures* **2022**, *41*, 1532–1545. [CrossRef]
39. Karmokar, T.; Mohyeddin, A.; Lee, J.; Paraskeva, T. Concrete cone failure of single cast-in anchors under tensile loading. *Eng. Struct.* **2021**, *243*, 112615. [CrossRef]
40. Helene, P.; Terzian, P. *Manual de Dosagem e Controle do Concreto*; PINI: São Paulo, Brazil, 1993; p. 349.
41. Fédération Internationale du Béton. *FIB Model Code for Concrete Structures*; FIB: Lausanne, Switzerland, 2010; Volume 2013, p. 402.
42. Takiguchi, K.; Harada, R.; Ishizeki, K. Pull out Strength an Anchor Bolt Embedded in Cracked Concrete. In Proceedings of the 15th International Conference on Structural Mechanics in Reactor Technology, Seoul, Republic of Korea, 15–20 August 1999; pp. 305–310.
43. Yoon, Y.S.; Kim, H.S.; Kim, S.Y. Assessment of fracture behaviors for CIP anchors fastened to cracked e uncracked concrete. *Int. J. Concr. Struct. Mater.* **2001**, *13*, 33–41.


**Disclaimer/Publisher's Note:** The statements, opinions and data contained in all publications are solely those of the individual author(s) and contributor(s) and not of MDPI and/or the editor(s). MDPI and/or the editor(s) disclaim responsibility for any injury to people or property resulting from any ideas, methods, instructions or products referred to in the content.